



This is the accepted manuscript made available via CHORUS, the article has been published as:

Two-band superconductivity in doped SrTiO₃ films and interfaces

R. M. Fernandes, J. T. Haraldsen, P. Wölfle, and A. V. Balatsky

Phys. Rev. B **87**, 014510 — Published 22 January 2013

DOI: [10.1103/PhysRevB.87.014510](https://doi.org/10.1103/PhysRevB.87.014510)

Two-band superconductivity in doped SrTiO₃ films and interfaces

R. M. Fernandes,^{1,2} J. T. Haraldsen,^{2,3} P. Wölfle,⁴ and A. V. Balatsky^{2,3,5}

¹*Department of Physics, Columbia University, New York, New York 10027, USA*

²*Theoretical Division, Los Alamos National Laboratory, Los Alamos, NM, 87545, USA*

³*Center for Integrated Nanotechnologies, Los Alamos National Laboratory, Los Alamos, NM 87545, USA*

⁴*Institute for Condensed Matter Theory and Institute for Nanotechnology, Karlsruhe Institute of Technology, D-76128 Karlsruhe, Germany*

⁵*NORDITA, KTH Royal Institute of Technology and Stockholm University, Roslagstullsbacken 23 106 91 Stockholm, Sweden*

We investigate the possibility of multi-band superconductivity in SrTiO₃ films and interfaces using a two-dimensional two-band model. In the undoped compound, one of the bands is occupied whereas the other is empty. As the chemical potential shifts due to doping by negative charge carriers or application of an electric field, the second band becomes occupied, giving rise to a strong enhancement of the transition temperature and a sharp feature in the gap functions, which is manifested in the local density of states spectrum. By comparing our results with tunneling experiments in Nb-doped SrTiO₃, we find that intra-band pairing dominates over inter-band pairing, unlike other known multi-band superconductors. Given the similarities with the value of the transition temperature and with the band structure of LaAlO₃/SrTiO₃ heterostructures, we speculate that the superconductivity observed in SrTiO₃ interfaces may be similar in nature to that of bulk SrTiO₃, involving multiple bands with distinct electronic occupations.

I. INTRODUCTION

The nature of multi-band superconductivity has been the subject of intense experimental^{1,2} and theoretical³⁻⁷ debate for decades. In the mid-1960s, specific heat measurements found evidence of multiple superconducting gaps in some elemental superconductors, such as Nb and V. More recently, multi-band superconductivity has been found in compounds displaying relatively high transition temperatures T_c : the magnesium diborides, with $T_c \approx 39\text{K}$ ¹⁰, and the iron pnictides, with T_c up to 56K ¹¹⁻¹⁶. While the superconducting states in these two classes of materials have significantly different microscopic structures, many of their thermodynamic properties display common signatures associated with the existence of multiple gaps. Such features encompass the temperature dependence of the specific heat and of the penetration depth, as well as the multiple-peak structure in tunneling spectroscopy.

Some of these characteristic multi-gap features have been observed in a lesser investigated material, electron-doped SrTiO₃ (STO). Indeed, oxygen-deficient STO possesses a superconducting state below $T_c \approx 0.3 - 0.4\text{K}$ ^{1,9}. Remarkably, tunneling measurements by Binnig *et al.*¹ in Nb-doped STO in the early 1980s found two peaks in the local density of states beyond a certain electronic density, providing strong evidence for multi-band superconductivity. More interestingly, the appearance of a second superconducting gap is correlated with a sudden increase in T_c , which can reach values up to 0.7K . Band structure calculations on Nb-doped STO also finds that near the electronic concentration where T_c is maximum, an additional electron-like band crosses the Fermi level^{8,10}.

Besides bulk STO, the recently discovered heterostructures of LaAlO₃/SrTiO₃ (LAO/STO) also display superconductivity up to $T_c \sim 0.2\text{K}$ ^{21,22}, which can be enhanced to $0.3 - 0.4\text{K}$ by the application of an electric field^{23,24}. This is surprisingly close to the aforementioned T_c value in bulk STO. Recent experiments have also found strong evidence that the maximum T_c in the heterostructures is achieved once an extra electron band becomes occupied¹⁷. In view of the early experiments by Binnig *et al.*¹, it is tempting to trace an analogy between superconductivity in bulk STO and in the LAO/STO heterostructures. Thus, the understanding of the multi-band superconducting state in electron-doped STO may be relevant for the ongoing debate on the nature of the superconducting LAO/STO heterostructures.

In both systems - bulk STO and LAO/STO interfaces - the origin and mechanism of the SC state is still an open issue. Most of the studies, however, have employed a single-band approach^{10,25-28}. In this paper, we do not discuss the origin of the SC state. We instead use a mean-field phenomenological two-dimensional model to focus on the consequences and signatures of multi-band superconductivity in these systems for varying electronic

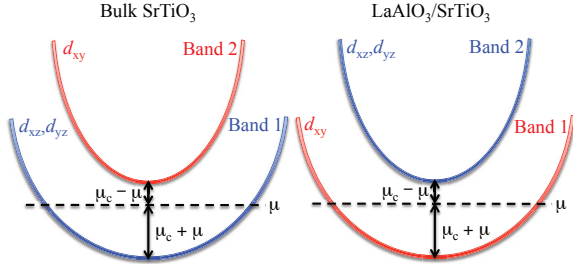


Figure 1: (Color Online) A general illustration of the two band model as applied to bulk STO (left panel) and LAO/STO (right panel). For STO, the d_{xz}/d_{yz} (band 1) crosses the Fermi level and the bottom of the d_{xy} (band 2) is located above the Fermi level by $\mu_c - \mu$. In the case of LAO/STO interface, orbital reconstruction switches the position of the bands.

concentration. Therefore, our approach is most relevant for thin films of doped STO and interfaces of STO with other systems that may provide negative charge carriers, such as LaAlO₃ and interfacial oxide gel²⁰.

In our model, motivated by first-principle calculations^{8,10}, the $d_{xz,yz}$ and d_{xy} orbitals form two electron bands such that, in the weakly doped compound, only one of them crosses the Fermi level (see Fig. 1). As the system is doped with negative charge carriers and the chemical potential μ shifts upwards, the second band crosses the Fermi level, causing important changes in the SC properties of the material. We calculate T_c , the gap functions, and the local density of states (LDOS) for different electronic concentrations, and compare our results with the tunneling experiments by Binnig *et al.* in Nb-doped STO¹. Such a comparison demonstrates that an attractive *intra-band* (*intra-orbital*) pairing interaction dominates over the *inter-band* (*inter-orbital*) pairing, in contrast to other recently found multi-band superconductors, such as the iron pnictides.

Although small, the inter-band coupling causes a sharp increase of T_c when the second band is occupied at $\mu = \mu_c$, and also enhances both gap functions, with the gap in the initially unoccupied band increasing faster than the gap in the initially occupied band. As a result, although for the undoped system these gaps have very different orders of magnitude, beyond $\mu = \mu_c$ they achieve comparable values, being manifested in the partial gaps as functions of μ and T (Fig. 3(a)). Our results are independent of the character of the inter-band interaction: for an attractive (repulsive) interaction, the gaps on two bands have the same (opposite) signs, but the thermodynamic properties discussed here remain the same. We also discuss possible connections with STO interfaces, proposing tunneling experiments on both the LAO/STO heterostructures and STO thin films to shed light on the superconducting state of these heterostructures. Finally, we discuss the importance of the dimensionality, arguing that most of the sharp features observed at $\mu = \mu_c$ in the two-dimensional model may be smoothed out by three-dimensional band dispersions.

Our paper is organized as follows: in Section II we formulate and solve our two-dimensional two-band model, discussing how T_c and the gap functions change as the chemical potential is varied. In Section III, we calculate the LDOS corresponding to the two-band model, comparing our results to the experiments of Binnig *et al.*¹. The effects of three-dimensionality are discussed in Section IV, and our concluding remarks are presented in Section V.

II. TWO-DIMENSIONAL TWO-BAND MODEL

A. Formulation of the model

First-principle calculations^{8,10} reveal that the band structure of bulk STO near the Fermi level is composed

of the Ti t_{2g} orbitals d_{xz} , d_{yz} , and d_{xy} . Due to the spin-orbit coupling, there is a splitting of $2\mu_c \sim 20 - 30$ meV between the $d_{xz/yz}$ and d_{xy} orbitals, with the latter having a larger onsite energy than the former. There is also another splitting between the d_{xz} and d_{yz} orbitals, which is however one order of magnitude smaller than μ_c . Here, we will neglect this extra splitting and consider an effective “heavy” degenerate $d_{xz/yz}$ electron-like band 1, whose bottom is located $\mu_c + \mu$ below the Fermi level, and a “light” electron-like d_{xy} band 2, whose bottom is located $2\mu_c$ above the bottom of the band 1 (see Fig. 1(a)). Notice that in the LAO/STO interfaces (shown in Fig. 1(b)), there is an orbital reconstruction that shifts the d_{xy} band below the $d_{xz/yz}$ ¹⁸. While this will change the possible orbital occupations of the electrons, the effective two-band model considered here is still representative of the system.

Introducing the electronic creation operators $c_{a,\mathbf{k}\sigma}^\dagger$, with band index a , momentum \mathbf{k} , and spin σ , we have the following interacting Hamiltonian in the pairing (particle-particle) channel:

$$H = \sum_{a,\mathbf{k},\sigma} (\varepsilon_{a,\mathbf{k}} - \mu) c_{a,\mathbf{k}\sigma}^\dagger c_{a,\mathbf{k}\sigma} + \sum_{a,b,\mathbf{k},\mathbf{k}'} V_{ab,\mathbf{k}\mathbf{k}'} c_{a,\mathbf{k}\uparrow}^\dagger c_{a,-\mathbf{k}\downarrow}^\dagger c_{b,-\mathbf{k}'\downarrow} c_{b,\mathbf{k}'\uparrow} + \text{h.c.} \quad (1)$$

where $\varepsilon_{a,\mathbf{k}}$ gives the band dispersion $\varepsilon_{1,k} = k^2/2m_1 - \mu_c$, $\varepsilon_{2,k} = k^2/2m_2 + \mu_c$, μ is the chemical potential, and $V_{ab,\mathbf{k}\mathbf{k}'}$ are the pairing interactions. Hereafter, we assume them to be momentum-independent, i.e. we consider s-wave SC states and for convenience choose the zero of energy to be at the midpoint between the two energy band minima. Furthermore, we consider that the pairing involves only states near the Fermi level, yielding the mean-field 2×2 system of gap equations:

$$\Delta_i = - \sum_{j=1}^2 \rho_j V_{ij} \Delta_j \int_{\mu_j}^W d\xi \frac{\tanh\left(\frac{\sqrt{\xi^2 + \Delta_j^2}}{2T}\right)}{2\sqrt{\xi^2 + \Delta_j^2}} \quad (2)$$

Here, W is the upper cutoff of the interaction, Δ_i are the SC gaps, ρ_i are the density of states at the Fermi level (in 2D the DOS is assumed to be independent of energy), $\mu_1 = -\mu - \mu_c$ is the position of the bottom of the electron-band 1, and $\mu_2 = \mu_c - \mu$ is the position of the bottom of the second band. For simplicity, we will discuss our results in terms of the dimensionless coupling constants $\lambda_{ij} = -\rho_i V_{ij}$. We assume $V_{21} = V_{12}$ and therefore $\lambda_{21} = (\rho_2/\rho_1)\lambda_{12}$.

From Eqs. (2) it is straightforward to obtain T_c . One linearizes the gap equations and calculates their largest eigenvalue, which equals 1 at T_c . This procedure yields the implicit equation:

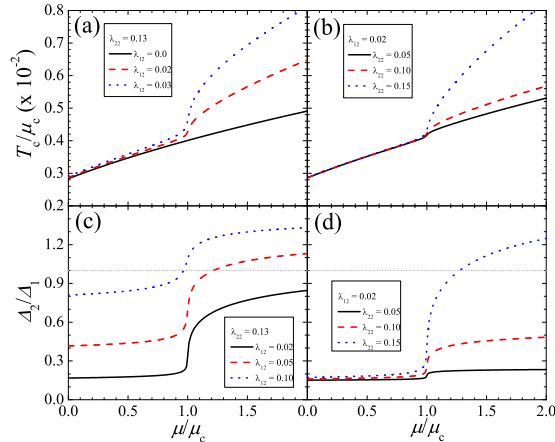


Figure 2: (Color Online) (a-b) Superconducting transition temperature T_c and (c-d) the $T = 0$ ratio of the gap as a function of chemical potential for various values of λ_{12} and λ_{22} . The light gray dotted line refers to $\Delta_2/\Delta_1 = 1$. Note, the gap of the second band is finite at all doping, but it is significantly smaller for $\mu < \mu_c$. In all panels, $\lambda_{11} = 0.14$.

$$1 = \left(\frac{\lambda_{11}I_1(\mu) + \lambda_{22}I_2(\mu)}{2} \right) + \sqrt{\left(\frac{\lambda_{11}I_1(\mu) - \lambda_{22}I_2(\mu)}{2} \right)^2 + \kappa\lambda_{12}^2I_1(\mu)I_2(\mu)} \quad (3)$$

where $\kappa \equiv \rho_2/\rho_1$ is the ratio between the density of states of the two bands at the Fermi level and $I_a(\mu)$ are implicit functions of $T_c \equiv 1.13W e^{-1/\lambda_c}$:

$$I_1(\mu) = \frac{1}{\lambda_c} + \frac{1}{2} \ln \left(\frac{\mu + \mu_c}{W} \right) \quad (4)$$

$$I_2(\mu) = \frac{\theta(\mu)}{2} \left[\frac{1}{\lambda_c} + \text{sign}(\mu - \mu_c) \int_0^{\frac{|\mu - \mu_c|}{2T_c}} dx \frac{\tanh x}{x} \right]$$

We note that $T_c \ll \mu_c \ll W$, which justifies the use of the log functions above. The last term in $I_2(\mu)$ is the one responsible for the changes in T_c as the second band crosses the Fermi level. In particular, very close to the point $\mu = \mu_c$, this function has a linear dependence on $\mu - \mu_c$, whereas far from this point, it behaves as the logarithm of $\mu - \mu_c$. We can also obtain the gap functions Δ_i from Eqs. (2) in a straightforward way. For $T = 0$, we obtain simple algebraic equations for Δ_{i0} . For non-zero $T < T_c$, one has to solve the self-consistent gap equations numerically.

Multi-band gap equations such as (2) have been investigated in the past in the context of different compounds, such as iron pnictides and MgB₂. Here, our interest is an

aspect of these gap equations that has not been as widely investigated^{30,35}, namely, the evolution of the solutions of the gap equations as a function of the chemical potential - particularly near the point where the second band starts to be occupied, $\mu = \mu_c$.

B. Results for T_c and Δ_i

We first need to discuss the values of the parameters that describe the electron-doped STO compounds. First, we note that the two bands have different orbital content, i.e. band 1 is composed of the $d_{xz/yz}$ orbitals, whereas band 2 is composed of d_{xy} orbitals. Since intra-orbital interactions are typically larger than inter-orbital interactions, we expect the intra-band pairing to be larger than the inter-band pairing, i.e. $|\lambda_{ii}| \gg |\lambda_{i \neq j}|$. As we will show below, this gives results in agreement with the experimental observations of Binnig *et al.*

Under these conditions, SC only appears for attractive intra-band interactions, $\lambda_{ii} > 0$, regardless of the sign of λ_{12} , since only λ_{12}^2 appears in the equation (3) for T_c . The sign of the inter-band coupling λ_{12} , however, affects the structure of the SC state, as the eigenvector that diagonalizes the linearized form of Eqs. (2) is such that $\text{sign}(\Delta_1\Delta_2) = \text{sign}(\lambda_{12})$. Thus, for $\lambda_{12} > 0$ (attractive inter-band interaction $V_{12} < 0$), Δ_1 and Δ_2 have the same sign (the so-called s^{++} state), whereas for $\lambda_{12} < 0$ (repulsive inter-band interaction $V_{12} > 0$), Δ_1 and Δ_2 have opposite signs (the s^{+-} state)³⁰. Since the SC free energy depends only on $\lambda_{12}\Delta_1\Delta_2$, the thermodynamic properties discussed in this paper do not depend on the relative sign between Δ_1 and Δ_2 . Therefore, we set $\lambda_{12} > 0$, but it is possible that STO is an unconventional s-wave superconductor with s^{+-} structure.

In Fig. 2, we present the enhancement of T_c as well as the ratio between the zero-temperature gaps Δ_{20}/Δ_{10} as a function of μ/μ_c for several different values of λ_{12} and λ_{22} , with $\lambda_{11} = 0.14$ fixed. Since band 2 is lighter than band 1, we have $\rho_2 = (m_2/m_1)\rho_1 = 0.4\rho_1$, in accordance with band structure calculations⁸. For the upper-cutoff W , we set $W = 10\mu_c$, and we consider $\lambda_{11} \approx \lambda_{22} \ll 1$ as well as $\lambda_{12} \ll \lambda_{ii}$, as discussed above. As it is shown in the figure, even when the inter-band pairing is small, the occupation of the second band at $\mu = \mu_c$ is marked by a sharp increase in T_c and by an enhancement in the zero-temperature gaps Δ_{10} and Δ_{20} . While for $\mu < \mu_c$ the gap Δ_{10} is significantly larger than Δ_{20} , for $\mu > \mu_c$ they become of similar magnitudes. The complete temperature behavior of the gap functions is shown in Fig. 3(a), which corresponds roughly to two BCS-like curves.

If we considered a larger inter-band interaction λ_{12} , then we would have obtained a larger enhancement of T_c at $\mu = \mu_c$, but the gap function Δ_{20} would be much closer to Δ_{10} even for $\mu < \mu_c$ (shown in Fig. 2(a) and (c)). Meanwhile, the tunneling experiments of Binnig *et al.*¹ suggest instead that Δ_{20} is considerably smaller than

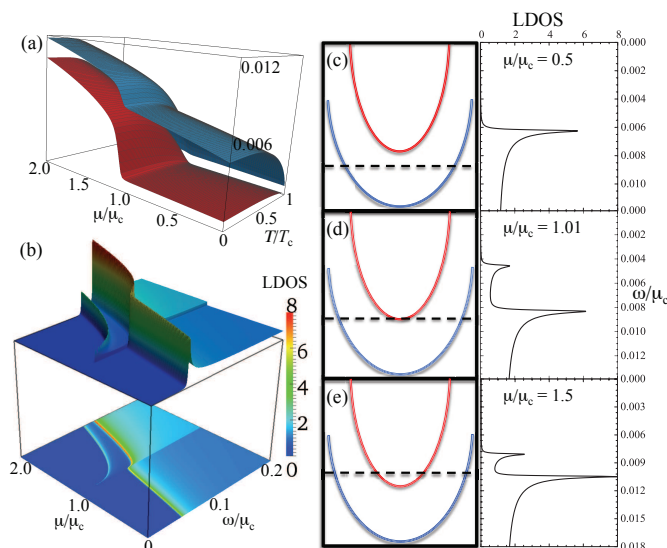


Figure 3: (Color Online) (a) Superconducting gap as a function of chemical potential and temperature, displaying the standard BCS temperature dependence. (b) Calculated LDOS for the two-band model as function of increasing chemical potential and energy. (c)-(e) The chemical potential levels with respect to the two bands (left) and the calculated LDOS for the two-band model for $\mu/\mu_c =$ (c) 0.5, (d) 1.01, and (e) 1.5 and for the set of parameters $\lambda_{11} = 0.14$, $\lambda_{22} = 0.13$, and $\lambda_{12} = 0.02$

Δ_{10} near $\mu = \mu_c$. Conversely, if we considered a smaller intra-band interaction $\lambda_{22} \ll \lambda_{11}$, then the enhancement of T_c at $\mu = \mu_c$ would be rather weak, in disagreement with the same data. Therefore, unless some fine-tuning is claimed, our results put important constraints on the character of the multi-band SC of electron-doped STO, as it appears to be dominated by attractive intra-band pairing interactions and weaker inter-band pairing.

Note that this situation is the opposite of other multi-band superconductors, such as the iron pnictides. These materials have a much larger repulsive inter-band interaction $\lambda_{12}^2 \gg \lambda_{11}\lambda_{22}$ enhanced by spin fluctuations, which gives rise to a sign-reversal s^{+-} state^{29,30}. Contrary to the iron pnictides, in STO the SC state is not near other electronic ordered states whose fluctuations can enhance λ_{12} .

III. TUNNELING SPECTRUM

The existence of two SC gaps has important implications for several thermodynamic quantities. For instance, two-gap superconductivity can be inferred from the temperature dependence of the specific heat and penetration depth. Yet, the most direct probe for multi-gap superconductivity is the local density of states (LDOS), which can be measured via tunneling spectroscopy.

Within our two-band model, the total LDOS $N(\omega)$ is the sum of the contributions from each band:

$$N(\omega) = -\frac{1}{\pi} \text{Im} \sum_{\mathbf{k}} [\nu_1 G_{11}(\omega, \mathbf{k}) + \nu_2 G_{22}(\omega, \mathbf{k})] \quad (5)$$

where $\nu_{1,2}$ denotes the degeneracy of the band. Within the mean field approximation each Green's function takes the BCS form $G_{jj} = (\omega + \xi_j(\mathbf{k})) / [\omega^2 - \xi_j^2(\mathbf{k}) - \Delta_j^2]$ with the respective gaps from Eq. 2. By replacing the summation over momenta by an integration over energies, the LDOS can be calculated analytically, yielding

$$N(\omega) = \text{Re} \left[\sum_j \frac{(\omega + i\eta + c_j) \rho_j(c_j) + (\omega - c_j) \rho_j(-c_j)}{2c_j} \right] \quad (6)$$

where ρ_j are the density of states of each band, $c_j = \sqrt{(\omega + i\eta) - \Delta_j^2}$, and η provides a small width to simulate experimental measurements. For the two-dimensional model considered so far, ρ_j are constants.

Using the $T = 0$ gaps obtained from the solution of Eqs. (2), we calculate $N(\omega)$. We observe two different behaviors, as shown in Fig. 3(b). For $\mu < \mu_c$, $N(\omega)$ has a sharp peak near $\omega = \Delta_{10}$, and the smaller gap Δ_{20} shows no noticeable signature. This is due to the fact that this gap is not open at the Fermi level, but at an energy near the bottom of the second band $\mu_c - \mu \gg \Delta_{20}$. We note that the LDOS has a clear increase at $\omega = \mu_c - \mu$ due to the additional contribution of the states coming from the second band. Only when $\mu_c - \mu \sim \Delta_{20}$, we see a weak signature of the second gap at energies slightly larger than Δ_{10} , where a clear peak is still observed.

For $\mu > \mu_c$, after the second band crosses the Fermi level, the second gap gives rise to a smaller peak at energies lower than the first peak, since $\Delta_{20} < \Delta_{10}$. As μ increases, this peak becomes larger and moves closer to the peak coming from the first-band gap. Eventually these two peaks become difficult to distinguish, since the gaps become comparable in magnitude. As a result, the LDOS has a sharp peak preceded by a shoulder-like feature (shown in Fig. 3(c)-(e)). These general features of the LDOS spectrum are in good agreement with the tunneling data of Ref.¹. We also point that the sharp peaks in the LDOS as the bands cross the Fermi level are comparable to the superconducting shape resonances that have been observed in films, quantum stripes, and nanowires.³¹⁻³⁵

IV. THREE-DIMENSIONAL CASE

So far we have focused on the 2D case, which is most relevant to STO thin films, interfaces, or probes sensitive to surface states, such as the tunneling experiments by Binnig *et al.*¹. In the bulk STO material, the 3D dispersion gives rise to a density of states $\rho(\xi) \propto \sqrt{\xi}$, which is expected to smoothen the sharp features observed in T_c

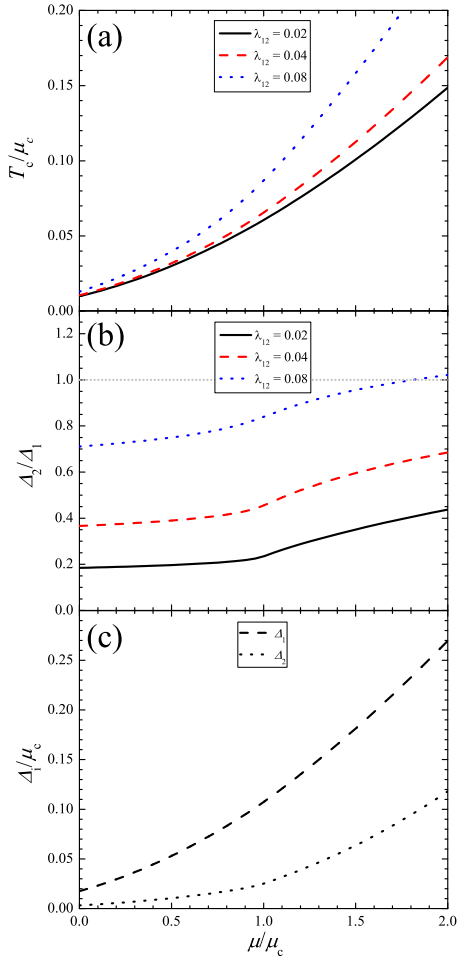


Figure 4: (Color Online) Calculations for the 3D two-band model as function of chemical potential for $\lambda_{11} = 0.14$ and $\lambda_{22} = 0.13$. We present T_c (a) and Δ_2/Δ_1 (b) for $\lambda_{12} = 0.02, 0.04$, and 0.08 . The light gray dotted line in (b) across $\Delta_2/\Delta_1 = 1$ denotes the point at which the second gap crosses the first gap. The individual energy gaps (Δ_i) for $\lambda_{12} = 0.02$ are shown in (c).

and Δ_{i0} at $\mu = \mu_c$. Nevertheless, as we will show in this section, the enhancement of T_c and Δ_{i0} at $\mu = \mu_c$ is still present.

We continue to assume parabolic bands. Then, the density of states of each band is given by $\rho_i = \rho_{i,0} \sqrt{\epsilon + \mu \pm \mu_c}$ and the gap equations are changed accordingly to:

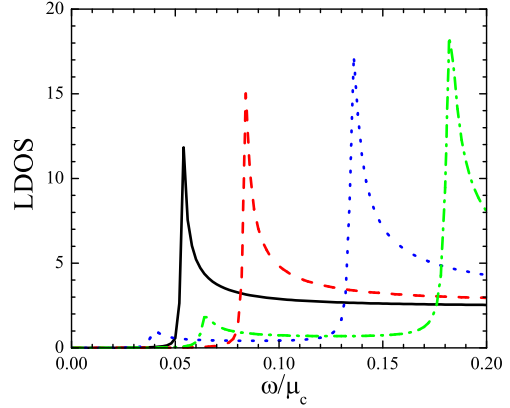


Figure 5: (Color Online) Calculated LDOS for the weakly coupled 3D two-band model as a function of ω/μ_c for $\mu/\mu_c = 0.5$ (solid-black), 0.8 (dashed-red), 1.2 (dotted-blue), 1.5 (dash-dotted-green). Here, we use the parameters $\lambda_{11} = 0.14$, $\lambda_{22} = 0.13$, $\lambda_{12} = 0.02$ and $\kappa = 0.4$.

$$\Delta_i = - \sum_{j=1}^2 \rho_{j,0} V_{ij} \Delta_j \times \int_{\mu_j}^W d\xi \frac{\sqrt{\epsilon + \mu \pm \mu_c}}{2\sqrt{\xi^2 + \Delta_j^2}} \tanh\left(\frac{\sqrt{\xi^2 + \Delta_j^2}}{2T}\right) \quad (7)$$

The solution of this system of equations is straightforward. In Fig. 4, we show the detailed behavior of the 3D two-band model as function of the chemical potential for $\lambda_{11} = 0.14$ and $\lambda_{22} = 0.13$ (the same parameters as in the 2D case). The evolution of T_c does produce an ‘‘upturn’’ around $\mu = \mu_c$, as shown in Fig. 4(a). The ratio of the gaps, presented in Fig. 4(b), displays a kink as the second band is populated. However, as shown in Fig. 4(c), the individual energy gaps display a distinct increase. This is consistent with the data observed by Binnig *et al*¹, where T_c and the gaps clearly increase as function of the chemical potential. The T_c data in Binnig *et al*¹ shows a slight kink as the second band becomes populated. The 3D model does not explain this slight kink and may indicate the presence of a 2D band structure from surface states. Therefore, we conclude that a two dimensional model is more accurate to describe the STO systems and may be the leading cause for the creation of a 2D electron gas at the interface of LAO and STO.

For completeness, we also calculate the local density of states (LDOS) resulting from the three-dimensional, two-band model. The LDOS is also given by Eq. (6), but with the appropriate energy-dependent density of states ρ_i . Figure 5 shows the results, with the LDOS plotted as a function of ω/μ_c for $\mu/\mu_c = 0.5, 0.8, 1.2, 1.5$. The

behavior is similar to the one observed by Binnig *et al.* in Ref.¹, where the population of the second band produces a small lower-frequency shoulder and an increase in the LDOS.

V. CONCLUSIONS

The observation of multiple gap structures in the tunneling spectrum of electron-doped bulk STO¹ is a well known fact, yet it has been largely overlooked in the discussion on the origin of superconductivity in both doped STO and LAO/STO interfaces. Motivated by this observation we proposed a multi-band model for superconductivity in electron-doped STO. The *d*-band manifold is split into two d_{xy} and $d_{xz/yz}$ bands with a splitting of around 10 meV before doping. We show that with increasing electronic occupation, the higher *d*-band(s) become occupied, engaging an additional source of electrons in the pairing. The onset of the occupation of the higher bands results in an increased DOS and pairing condensate gain, which in turn results in a sharp increase in T_c and in the SC gap in the second band. Comparing to experiments, we find the primary source of pairing to be the intra-band coupling $\lambda_{11,22}$ with smaller inter-band Josephson coupling $\lambda_{12} \ll \lambda_{11,22}$. Depending on the sign of the inter-band coupling, the SC gaps on the two bands can have the same or opposite signs, resulting in either s^{++} or s^{+-} SC states. Although our results were motivated by bulk STO, the fact that T_c in the LAO/STO interfaces is very close to the T_c of electron-doped STO⁹, and the observation that the maximum T_c of the het-

erostructure takes place when a second *d*-band becomes occupied^{25,26}, we suggest that the same multi-band effects may take place in the oxide interfaces. Of course, in the heterostructures, the breaking of inversion symmetry at the surface may lead to additional contributions to T_c , not considered in our model³⁶.

To test our proposal, we suggest to use simple direct spectroscopy in the SC state of doped STO thin films and LAO/STO interfaces, such as scanning tunneling microscopy or planar tunneling. Both probes would reveal the existence of a two gap structure if indeed superconductivity is a two-band phenomena in these systems. The observation of two band features would likely be possible only in a clean limit when scattering will not wash away features of the weaker gap. Given the weak-coupling nature of this two-band system, we also mention a possibility of novel physics in the observable effect of hidden criticality and the possible difference in the superconducting length scales.^{37,38}

We are grateful to Q. Jia, P. Hirschfeld, H. Hwang, T. Kopp, J. Mannhart, I. Schuller, J. Triscone, S. Trugman, J.X. Zhu for useful discussions and criticism. This work was supported by Los Alamos and Aspen Center for Physics. Los Alamos National Laboratory, an affirmative action equal opportunity employer, is operated by Los Alamos National Security, LLC, for the National Nuclear Security Administration of the U.S. Department of Energy under contract DE-AC52-06NA25396. R.M.F. and A.V.B. were supported by the NSF Partnerships for International Research and Education (PIRE) program OISE-0968226.

-
- ¹ G. Binnig, A. Baratoff, H. E. Hoening, and J. G. Bednorz, Phys. Rev. Lett. **45**, 1352 (1980).
- ² M. Iavarone, G. Karapetrov, A. E. Koshelev, W. K. Kwok, G. W. Crabtree, D. G. Hinks, W. N. Kang, E.-M. Choi, H. J. Kim, H.-J. Kim, and S. I. Lee, Phys. Rev. Lett. **89**, 187002 (2002).
- ³ H. Suhl, B. T. Matthias, and L. R. Walker, Phys. Rev. Lett. **3**, 552 (1959).
- ⁴ N. Schopohl and K. Scharnberg, Solid State Comm. **22**, 371 (1977).
- ⁵ M. Iskin and C. A. R. Sa de Melo, J. Low Temp. Phys. **149**, 29 (2007).
- ⁶ E. Babaev, J. Carlstrom, J. Garaud, M. Silaev, and J. M. Speight, Physica C **479**, 2 (2012).
- ⁷ J. Geyer, R. M. Fernandes, V. G. Kogan, and J. Schmalian, Phys. Rev. B **82**, 104521 (2010).
- ⁸ L. F. Mattheiss, Phys. Rev. B **6**, 4718 (1972).
- ⁹ C. S. Koonce, M. L. Cohen, J. F. Schooley, W. R. Hosler, and E. R. Pfeiffer, Phys. Rev. **163**, 380 (1967).
- ¹⁰ D. van der Marel, J. L. M. van Mechelen, and I. I. Mazin, Phys. Rev. B **84**, 205111 (2011).
- ¹¹ Y. Kamihara, T. Watanabe, H. Hirano, and H. Hosono, J. Am. Chem. Soc. **130**, 3296 (2008).
- ¹² G. F. Chen, Z. Li, D. Wu, G. Li, W. Z. Hu, J. Dong, P. Zheng, J.L. Luo, and N.L. Wang, Phys. Rev. Lett. **100**, 247002 (2008).
- ¹³ Z.-A. Ren, J. Yang, W. Lu, W. Yi, G.-C. Che, X.-L. Dong, L.-L. Sun, and Z.-X. Zhao, Mater. Res. Innovations **12**, 1 (2008).
- ¹⁴ P. Cheng, L. Fang, H. Yang, X. Zhu, G. Mu, H. Luo, Z. Wang, and H.-H. Wen, Sci. China Ser. G **51**, 719 (2008).
- ¹⁵ Q. Si and E. Abrahams, Phys. Rev. Lett. **101**, 076401 (2008).
- ¹⁶ M. Rotter, M. Tegel, and D. Johrendt, Phys. Rev. Lett. **101**, 107006 (2008).
- ¹⁷ A. Joshua, S. Pecker, J. Ruhman, E. Altman, and S. Ilani, arXiv:1110.2184
- ¹⁸ M. Salluzzo, J. C. Cezar, N. B. Brookes, V. Bisogni, G. M. De Luca, C. Richter, S. Thiel, J. Mannhart, M. Huijben, A. Brinkman, G. Rijnders, and G. Ghiringhelli, Phys. Rev. Lett. **102**, 166804 (2009).
- ¹⁹ J. Nagamatsu, N. Nakagawa, T. Muranaka, Y. Zenitani, and J. Akimitsu, Nature **410**, 63 (2001).
- ²⁰ K. Ueno, S. Nakamura, H. Shimotani, A. Ohtomo, N. Kimura, T. Nojima, H. Aoki, Y. Iwasa, and M. Kawasaki, Nature Materials **7**, 855 (2008).
- ²¹ N. Reyren, S. Thiel, A. D. Caviglia, L. Fitting Kourkoutis, G. Hammerl, C. Richter, C. W. Schneider, T. Kopp, A.-

- S. Rüetschi, D. Jaccard, M. Gabay, D. A. Muller, J.-M. Triscone, and J. Mannhart, *Science* **317**, 1196 (2007).
- ²² J. Heber, *Nature* **459**, 28 (2009).
- ²³ A. D. Caviglia, S. Gariglio, N. Reyren, D. Jaccard, T. Schneider, M. Gabay, S. Thiel, G. Hammerl, J. Mannhart, and J.-M. Triscone, *Nature* **456**, 624 (2008).
- ²⁴ C. Bell, S. Harashima, Y. Kozuka, M. Kim, B. G. Kim, Y. Hikita, and H. Y. Hwang, *Phys. Rev. Lett.* **103**, 226802 (2009).
- ²⁵ M. Huijben, A. Brinkman, G. Koster, G. Rijnders, H. Hilgenkamp, and D. H. A. Blank, *Adv. Mater.* **21**, 1665 (2009).
- ²⁶ S. Gariglio, N. Reyren, A. D. Caviglia, and J.-M. Triscone, *J. Phys.: Condens. Matter* **21**, 164213 (2009).
- ²⁷ P. Zubko, S. Gariglio, M. Gabay, P. Ghosez, and J.-M. Triscone, *Annu. Rev. Condens. Matter Phys* **2**, 141 (2011).
- ²⁸ J. A. Bert, B. Kalisky, C. Bell, M. Kim, Y. Hikita, H. Y. Hwang, and K. A. Moler, *Nature Physics* **7**, 767 (2011).
- ²⁹ for reviews, see D. C. Johnston, *Adv. Phys.* **59**, 803 (2010); J. Paglione and R. L. Greene, *Nature Phys.* **6**, 645 (2010). P. J. Hirschfeld, M. M. Korshunov, and I. I. Mazin, *Rep. Prog. Phys.* **74**, 124508 (2011); D. N. Basov and A. V. Chubukov, *Nature Phys.* **7**, 241 (2011); P. C. Canfield and S. L. Bud'ko, *Annu. Rev. Cond. Mat. Phys.* **1**, 27 (2010); H. H. Wen and S. Li, *Annu. Rev. Cond. Mat. Phys.* **2**, 121 (2011); A. V. Chubukov, *Annu. Rev. Cond. Mat. Phys.* **3**, 57 (2012); G. R. Stewart, *Rev. Mod. Phys.* **83** 1589 (2011).
- ³⁰ R. M. Fernandes and J. Schmalian, *Phys. Rev. B* **82**, 014521 (2010).
- ³¹ J. M. Blatt and C. J. Thompson, *Phys. Rev. Lett.* **10**, 332 (1963).
- ³² M. Yu, M. Strongin, and A. Paskin, *Phys. Rev. B* **14**, 996 (1978).
- ³³ A. Perali, A. Bianconi, A. Lanzara, and N. L. Saini, *Solid State Comm.* **100**, 181 (1996).
- ³⁴ A. A. Shanenko, M. D. Croitoru, and F. M. Peeters, *Phys. Rev. B* **75**, 014519 (2007).
- ³⁵ D. Innocenti, N. Poccia, A. Ricci, A. Valletta, S. Caprara, A. Perali, and A. Bianconi, *Phys. Rev. B* **82**, 184528 (2010).
- ³⁶ J. T. Haraldsen, P. Wölfle, and A. V. Balatsky, *Phys. Rev. B* **85**, 134501 (2012).
- ³⁷ L. Komendová, Yajiang Chen, A. A. Shanenko, M.V. Milosević, and F. M. Peeters, *Phys. Rev. Lett.* **108**, 207002 (2012).
- ³⁸ L. Komendova, M. V. Milosevic, A. A. Shanenko, and F. M. Peeters, *Phys. Rev. B* **84**, 064522 (2011).